Photon echo from free excitons in a CH₃NH₃PbI₃ halide perovskite single crystal

R. S. Nazarov [1] I. A. Solovev,[1] A. O. Murzin,[1] N. I. Selivanov,[1] J. Even [2] A. V. Emeline,[1] and Yu. V. Kapitonov [1,*]

[1]*Saint Petersburg State University, Physics faculty, 7/9 Universitetskaya Emb., St. Petersburg 199034, Russia*
[2]*Univ Rennes, INSA Rennes, CNRS, Institut FOTON - UMR 6082, 20, Avenue des buttes de Coesmes, F-35000 Rennes, France*

Halide perovskites show great potential for a variety of optoelectronic applications. The presence of robust exciton resonance in these materials makes them promising for use in information photonics. In this paper, we demonstrate the possibility of writing and delayed reading of the optical coherence in halide perovskite by the spontaneous (two-pulse) photon echo in MAPbI₃ (MA⁺ = CH₃NH₃⁺) lead-halide perovskite single crystal on picosecond time scales. The spectral and polarimetric measurements of the photon echo signal confirm the free excitonic origin of the excitation under study. Observed relatively long dephasing time, high exciton oscillator strength, and weakly pronounced excitation-induced dephasing make halide perovskites a promising media for applications.

I. INTRODUCTION

Manipulation of the optical coherence can be used to create information photonics devices. Photon echo (PE) can store the optical coherence in the material excitations and revive it upon request. Excitons and their complexes in epitaxial heterostructures are traditionally used as such excitations in practically important semiconductor materials [1–5]. In the last decade, two rising stars have appeared in the sky of excitonic materials: monolayers of transition metal dichalcogenides (TMDCs) [6–8] and halide perovskites [9,10].

Halide perovskites attracted sudden attention as efficient media for solar cell absorbers [11–13]. It progressively became apparent that in addition to high absorption these new ionic direct-gap semiconductors also have excellent emissivity. This is largely due to their defect tolerance—a unique feature of the band structure of halide perovskites [14,15]. The nature of the photoexcited species at room temperature in operating perovskite devices remained an open question [16]. On the one hand, excitons were considered stable at room temperature on the basis of Wannier-Mott exciton binding energies ranging from 37 to 50 meV in MAPbI₃ previously obtained using low-temperature magnetoabsorption spectroscopy [10,17–19]. On the other hand, the data on unexpectedly long diffusion lengths [20,21] argued against this.

This paradox was only resolved with a detailed experimental characterization of the Wannier-Mott exciton Rydberg series in MAPbI₃ [9]. These experiments demonstrated a significantly lower binding energy of the order of 16 meV at low temperature and down to a few meV at room temperature, in full agreement with earlier theoretical predictions [22]. Finally, studies of MAPbI₃ [23] and MAPbBr₃ [24] single crystals definitively demonstrated the existence of

Wannier-Mott exciton resonances, and attributed the previously observed resonances to bound excitons (BE) or additional low energy features depending on the sample preparation or film crystallinity. Accurate experimental characterization of free excitons (FE) is now available for almost all the 3D halide perovskites, including hybrid and inorganic compounds [25–27]. Excitonic effects are important in quantum dot based devices, bright LEDs designed for room temperature or for single photon or entangled photon quantum sources operating at low temperature.

FE are of great interest for photonics applications due to the enormous oscillator strength concentrated in a narrow spectral region and the strong nonlinearity of their optical response. The simplest experiment demonstrating the signal arising entirely due to nonlinearity is the four-wave mixing (FWM). In several works, FWM of MAPbI₃ polycrystalline thin films was studied [28–30]. Due to the large density of surface defects in such samples, only the subpicosecond dynamics was observed. The inhomogeneous broadening of transitions also limits the FWM spectroscopy applications. Similar FWM results were also obtained for ensembles of MAPbI₃ nanoplatelets [31] and polycrystalline thin films of 2D halide perovskite-like materials [32–34]. Subpicosecond PE was observed in MAPbI₃ single crystals [35].

The most suitable object for studying fundamental optical properties of halide perovskites are single crystals at cryogenic temperatures. In this case, both inhomogeneous and thermal broadening of material resonances are minimized, and spectroscopy works at full strength. It was with the use of single crystals of MAPbBr₃ perovskites that the Wannier-Mott nature of excitons was established in [24], where ground and excited states of free excitons were observed in the photoluminescence (PL) and reflectance spectra. Measurements of MAPbX₃ (X⁻ = Br⁻, I⁻) single crystals in a magnetic field provide such important parameters as exciton binding energies, reduced masses, g factors, and oscillator strengths
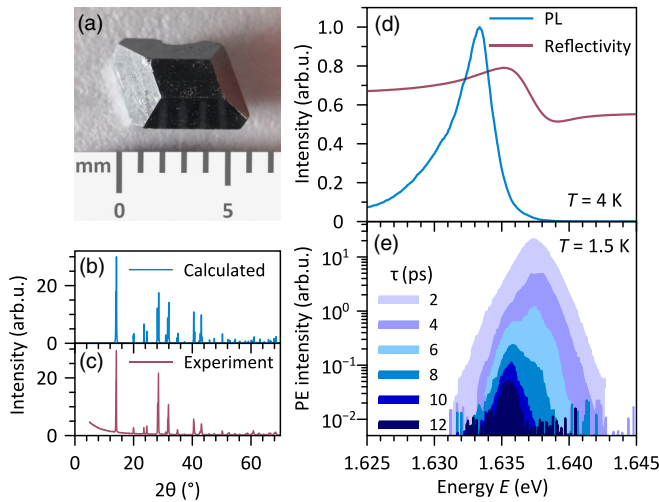
FIG. 1. (a) MAPbI$_3$ single crystal. Calculated (b) and experimental (c) XRD patterns for powdered MAPbI$_3$ single crystal. (d) PL (blue) and normal reflectance (red) spectra of the single crystal at T = 4 K. (e) Spectra of PE at $t = 2\tau$ for different delay times τ taken at T = 1.5 K (log scale).

[10]. These and other studies [36] also helped to support the energy diagram of excitonic transitions. We would like to mention that in a number of studies using exclusively PL as an optical method, the intense bound exciton (BE) emission line [37] was mistakenly identified as the FE transition, which can in fact only be observed in high-quality single crystals below broad BE signatures [23]. Indeed, the existence of low-temperature structural phase transitions in hybrid MAPbX$_3$ perovskites associated with structural distortions is promoting BE emission, especially in thin films. Moreover, recent studies show that the coherent evolution of electrons and holes at low temperature in MAPbI$_3$ films can be mainly explained as the result of both localized electrons and holes evolution [38]. We will provide additional arguments in favor of separating FE and BE spectral features.

Here we report for the observation of PE in halide perovskites in MAPbI$_3$ (MA$^+$ = CH$_3$NH$_3^+$) single crystal on picosecond time scales. The spontaneous PE signal is well resolved in angular, temporal, and spectral domains at T = 1.5 K. The spectral position and distinct polarimetric behavior of the PE signal allowed us to identify its origin as a FE transition in MAPbI$_3$ bulk. This conclusion was supported by PL and normal reflectance measurements. The PE of FE resonance shows the irreversible phase relaxation time T_2 = 8.2 ps, which tends to rise for lower-lying excitonic states due to the localization, and a weak tendency to fall for high light intensities due to the excitation-induced dephasing (EID).

II. RESULTS AND DISCUSSION

A. Crystal growth and characterization

MAPbI$_3$ single crystals were grown by the counterdiffusion-in-gel method [39–41] (see Sec. IV). Using this method, single crystals with a size of the order of several mm were obtained [Fig. 1(a)]. Powder x-ray diffraction (XRD) was used to prove the intended single-phase

perovskite structure. The experimentally obtained diffraction pattern [Fig. 1(b)] coincides with the one calculated based on the known MAPbI$_3$ crystal structure [42] [Fig. 1(c)].

B. Optical characterization

The optical characterization of the crystals was performed at a temperature of T = 4 K. Figure 1(d) shows PL and normal reflectance spectra. Reflectance is dominated by the FE resonance due to the concentration of the oscillator strength in this transition in direct-gap MAPbI$_3$ semiconductor at low temperatures. The PL spectrum shows a strong emission line at 1.633 eV [Fig. 1(d)]. Based on the Stokes shift this line was associated with BE state. Although the exact nature of these bound states is debatable, they are observed in the whole family of three-dimensional ABX$_3$ halide perovskites [23,24,37,43,44].

C. Four wave mixing measurements

FWM measurements were performed at a temperature of T = 1.5 K. The sample was excited by two 3 ps light pulses with wave vectors $\vec{k}_1$ and $\vec{k}_2$ close to the normal incidence and time delay τ between pulses [Fig. 2(a)]. The FWM signal was detected in the reflection geometry along the direction $\vec{k}_{\mathrm{FWM}} = (2\vec{k}_2 - \vec{k}_1)_\sigma$, where σ denotes reflection by the sample plane. The FWM signal amplitude P was obtained by the cross-correlation with the reference pulse. In the FWM setup P could be detected with temporal resolution and with the control of the polarization and intensity of the exciting pulses and the polarization of the detection. In this section, all experiments were carried out in colinear polarization of exciting pulses and detection. More details on the experimental setup could be found in Sec. IV.

At $\tau = 0$ the conventional FWM signal was detected at temporal position $t = 0$ (where t is counted from the first pulse arrival time) with maximum at $E = 1.638$ eV well aligned with FE resonance in reflectance spectrum. After the delay time was increased to $\tau = 12$ ps, the FWM signal maximum shifted to $t = 21$ ps [Fig. 2(b)]. The FWM direction of this signal and its pronounced temporal behavior with the signal maximum near $t = 2\tau$ means the spontaneous PE response. The temporal profile of this signal is determined by the inhomogeneous broadening of the excited ensemble and could be described by the Gaussian function $P \sim \exp(-\frac{4\ln(2)\,(t-2\tau)^2}{T_2^{*2}})$ [Fig. 2(b)] yielding the reversible phase relaxation time $T_2^* = 7.2$ ps.

Figure 3(a) shows the dependence of the temporal profile of the PE signal on τ. The signal is following the expected PE position at $t = 2\tau$ clearly and could be separated from the free polarization decay signal immediately following the 2nd pulse ($t = \tau$). The PE decay could be measured as the PE signal at $t = 2\tau$ [Fig. 2(c)]. This signal was fitted by the exponential decay $P \sim \exp(-\frac{2\tau}{T_2})$ yielding the irreversible phase relaxation time $T_2 = 8.2$ ps.

PE dependence on the 1st and 2nd pulses intensities up to 1600 mW do not show Rabi oscillations. This behavior is typical for states with a large oscillator strength, such as FE, in contrast, to BE and trions, where Rabi oscillations can be observed at much lower intensities [3,45]. The
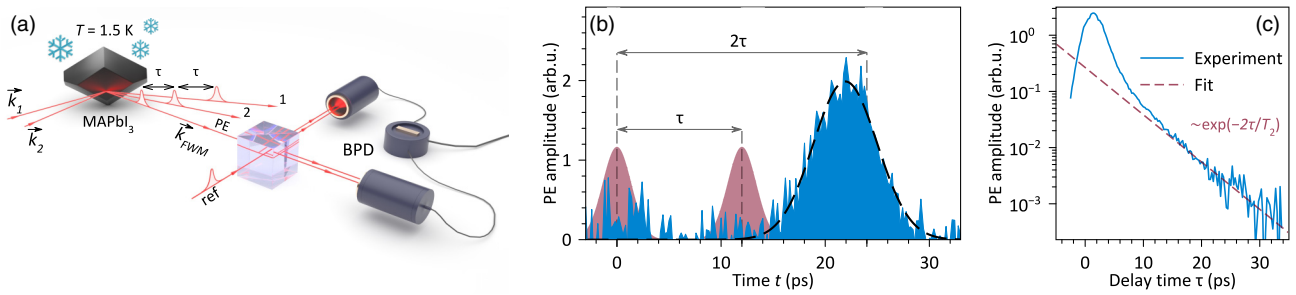
FIG. 2. (a) Schematic presentation of FWM setup. Two laser pulses (1 and 2) with wavevectors $\vec{k}_1$ and $\vec{k}_2$ excite the cooled MAPbI$_3$ crystal (black). Pulse 2 is delayed by τ time compared to the pulse 1. After an additional τ delay a new pulse emerges from the sample in the FWM direction $\vec{k}_{FWM}$. This signal is mixed with the reference pulse (ref) on a nonpolarized beamsplitter cube and detected by the balanced photodiode (BPD). Angles are exaggerated for clarity. (b) PE profile measured at $E = 1.6365$ eV. Red curves schematically represent laser pulses; blue curve: the signal detected in the $\vec{k}_{FWM}$ direction. Black dashed curve: Gaussian fit (see text) with $T_2^* = 7.2$ ps. (c) PE decay measured at $t = 2\tau$ and $E = 1.6365$ eV (blue curve). Red dashed curve: exponential decay fit with $T_2 = 8.2$ ps (log scale).

excitation-induced dephasing (EID) was observed as a decrease of the T_2 with pulses intensities growth. Figure 3(d) shows the dependence of the irreversible phase relaxation rate $\Gamma_2 = \frac{1}{T_2}$ on the 1st pulse intensity I_1. Dephasing is slowly growing with I_1 [Fig. 3(d)]. A similar weak EID was observed in [29].

Figure 1(e) shows the PE spectra measured for different τ. The spectral position of the PE signal coincides with the position of the FE determined from the reflectance spectrum. The redshift of the spectral maximum with increasing τ is a typical manifestation of T_2 increase for more localized exciton states. However, there is no signal at the BE spectral position, which is apparently due to its very low oscillator strength. Thus, we can conclude that the observed PE signal is related to the FE state.

D. Photon echo polarimetry

A distinctive feature of FE is the energy diagram, where the ground level is the ground ("vacuum") state of the crystal. Symmetry analysis for optical transitions in bulk AMX$_3$ halide perovskites with cubic symmetry (Pm-3m space group)

taking into account the spin-orbit coupling (SOC) leads to the following excited excitonic states [36]: lowest energy optically inactive singlet state ($J = 0$) and optically active threefold degenerate triplet state ($J = 1$) [Fig. 3(c)]. When the temperature is lowered from the room temperature the MAPbI$_3$ halide perovskite first transforms into tetragonal and then into orthorhombic symmetry, which is stable below ~ 161 K [46]. Such symmetry decrease induces the lifting of the degeneracy of the triplet state. The scale of the splitting for 3D bulk halide perovskites is usually below 0.5 meV [47], which is less than the excitonic resonance width (5 meV) and the spectral resolution of picosecond pulses in our experiment. In this regard, further, we will consider the absence of the degeneracy lifting.

The powerful method for the identification of the energy diagram of optical transitions is the PE polarimetry, which was originally proposed for gases [48], and has recently been successfully demonstrated for semiconductor heterostructures [49]. In this method, the two-pulse spontaneous PE is detected with the fixed linear polarization of the first pulse, and the second pulse linear polarization rotated by the angle φ with respect to the first pulse polarization. The co- and cross-linear
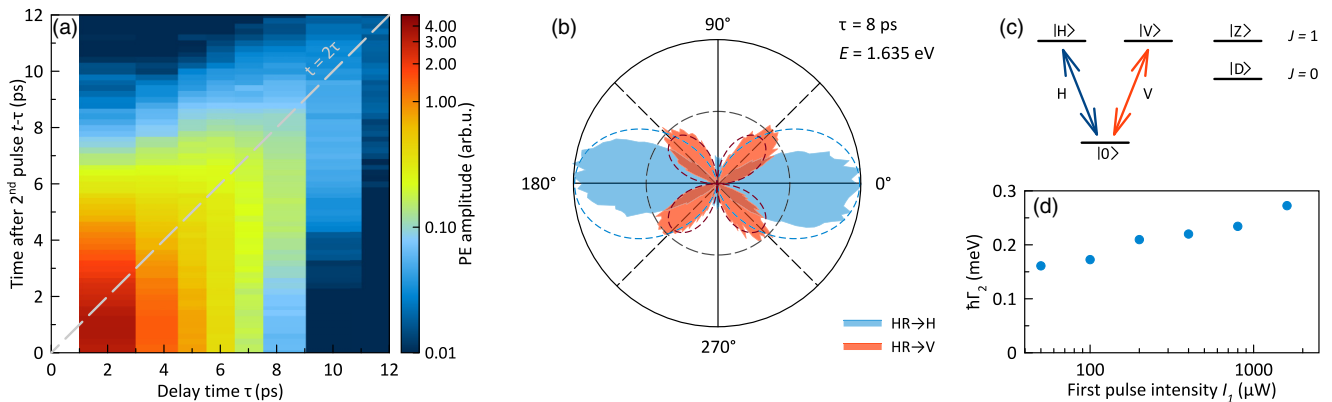

FIG. 3. (a) PE signal at different delay times τ and time after second pulse $t - \tau$ (log intensity scale). (b) Polar plots of PE signal measured at different angles between first and second pulses for HR $\rightarrow$ H (red) and HR $\rightarrow$ V (blue) polarization geometries. Dashed curves represent theoretically predicted signal behavior for FE. (c) Energy diagram of excitonic stated in MAPbI$_3$ crystal. (d) Irreversible phase relaxation rate Γ_2 for different intensities of the first pulse I_1 (log intensity scale).

detection with respect to the first pulse is carried out, thus leading to two polar plots. Analysis of these plots could be used to distinguish states with different energy diagrams such as excitons, trions [49], and biexcitons [35]. An important advantage of this method is that there is no need to apply an external magnetic field to the sample.

In our experiment, incident light is almost normal to the sample plane. In this case, for the cubic crystal symmetry, regardless of the orientation of the sample plane, it seems possible to choose a basis in which two states lie in this plane ($|H\rangle$ and $|V\rangle$), and the third is normal to it ($|Z\rangle$) [Fig. 3(c)]. We will assume that the orientation of states coincides with the horizontal (vertical) laboratory axis H (V). In this case the H-(V-) polarized light addresses the $|0\rangle \leftrightarrow |H\rangle$ ($|0\rangle \leftrightarrow |V\rangle$) transition. Since no other states are involved, the problem could be narrowed down to the three-level system including $|0\rangle$, $|H\rangle$ and $|V\rangle$ states. The PE polarimetric measurements can be represented as measurements in HR → H and HR → V geometries, where the first two letters denote polarizations of exciting pulses (where R represents the scan with φ from 0 to 2π), and the third one—the detection polarization, determined by the reference pulse.

Figure 3(b) shows the HR → H and HR → V polar plots for PE from the supposed FE state ($E = 1.635$ eV, $\tau = 8$ ps). Due to the same symmetry of optically addressed states, the theoretical consideration of the three-level system leads to the same result as in the case of quantum wells in the zinc blende structures [49,50]: $P_{HR\rightarrow H} \sim \cos(\varphi)^2$, $P_{HR\rightarrow V} \sim \sin(\varphi)\cos(\varphi)$ (see Sec. IV). This result also coincides with that obtained in [35]. The experimental data demonstrate excellent agreement with theoretical predictions [dashed lines in Fig. 3(b)], which is another confirmation of the excitonic nature of the resonance observed in PE.

III. SUMMARY

In summary, we have demonstrated the spontaneous PE signal formation in MAPbI$_3$ halide perovskite single crystal on picosecond time scales. PE spectroscopy and polarimetry prove the free excitonic origin of the observed material resonance. The observation of 8 ps dephasing time and a weakly pronounced EID effect proposes halide perovskites as a promising material for optical memory elements in the area of the information photonics.

IV. METHODS

A. Chemicals

Lead (II) iodide PbI$_2$ (99%, Sigma-Aldrich), hydroiodic acid HI (56% in H$_2$O, Iodobrom), hypophosphorous acid H$_3$PO$_2$ (50% in H$_2$O, Acros Organics), methylamine CH$_3$NH$_2$ (38% in H$_2$O, Lenreactiv) were used as received. Silica gel was prepared from sodium metasilicatecrystallohydrate solution Na$_2$SiO$_3$ · 9H$_2$O with the distilled water as solvent. To stabilize the hydroiodic acid, hypophosphorous acid was added to it in the 9:1 volume ratio.

B. Gel growth

A silica gel matrix was formed in a U-shaped glass tube (U tube). For the silica gel preparation, a required weight of Na$_2$SiO$_3$ · 9H$_2$O was dissolved in water to obtain a solution with the 0.6 M concentration of sodium metasilicate. This solution was added dropwise and with vigorous stirring to the hydrohalic acid with the 1:2 volume ratio. The prepared transparent sol was poured into the U tube with the 20 mm inner diameter. A sol-gel conversion took place for 48 hours, and a dense homogeneous silica gel was formed.

C. Perovskite single crystal formation

Solution of PbI$_2$ in hydroiodic acid with 1.2 M concentration was prepared. Solution of methylammonium iodide (MAI) with 1.2 M concentration was prepared by adding the methylamine solution to the hydroiodic acid. The PbI$_2$ solution was poured over the silica gel into one of the limbs of the U tube. A MAI solution was poured into another limb. The U tube was placed in a thermostat at T $= 35°$C. After 2–3 weeks the MAPbI$_3$ single crystals were nucleated in the gel and continued to grow. Fully grown crystals were mechanically removed from the gel, washed in the diluted solution of hydroiodic acid, and, after drying in the oven at 40°C, were used for further studies.

D. Structural characterization

Powder x-ray diffraction was recorded with a high-resolution x-ray diffractometer Bruker D8 Discover using a long focus x-ray tube CuKα anode. Reflected x-rays were detected using a solid position-sensitive detector LYNXEYE. Measurements were carried out at room temperature.

E. Optical characterization

MAPbI$_3$ single crystal was mounted in the closed-cycle helium cryostat Montana Instruments and cooled down to the temperature $T = 4$ K. The 10x Mitutoyo microlens was used to excite the sample and to collect the outgoing light. The custom-made spectrometer with the CCD array was used to capture spectra with a resolution below 0.1 meV. Normal reflectance was measured using a halogen lamp. The PL was excited by the Ti:Sapphire cw-laser tuned well above the MAPbI$_3$ band gap ($\lambda = 745$ nm).

F. Four-wave mixing

For FWM measurements MAPbI$_3$ single crystal was kept in the liquid helium at $T = 1.5$ K in the closed-cycle helium cryostat Cryogenics. The light beam from the Ti:Sapphire ps-pulsed laser Spectra-Physics Tsunami was split into three channels: the first and the second pulses were used to excite the sample, the reference pulse was used to perform the cross-correlation measurements of the PE signal. The measurements were carried out close to the normal geometry. The first and second pulses were focused on the sample in the 100 μm diameter area with angles of incidence differing by 0.5°. Removal of the incidence angle degeneracy provides the isolation of the PE signal in the $\vec{k}_{FWM}$ direction. PE signal and reference pulse were mixed on the nonpolarizing beamsplitter cube, and detected by the balanced photodetector Newport 2107. The cross-correlation signal was enhanced by the double synchronous detection with fast modulation at Δf

= 1 MHz frequency achieved by acousto-optic shifters introducing the frequency shift of the first and reference pulses by +80 MHz and −81 MHz correspondingly; and slow mechanical chopper modulation of the first pulse at 1.7 kHz frequency. Optical delay lines installed in the second pulse and reference pulse arms are used to detect the time-resolved FWM signal for different delay times between excitation pulses. Polarizers and half-wave plates were used to select excitation and detection polarizations.

G. Photon echo polarimetry

Let us consider the three-level system depicted in Fig. 3(c). The ground state $|0\rangle$ and the excited state $|H\rangle$ ($|V\rangle$) are coupled by the H- (V-) linear polarized light. This system could be described by the density matrix ρ, where ρ_{11} and ρ_{22} matrix elements representing populations of excited states $|H\rangle$ and $|V\rangle$ correspondingly, and $\rho_{01} = \rho_{10}^*$ and $\rho_{02} = \rho_{20}^*$ are matrix elements responsible for optical polarizations. The temporal evolution of the system could be found using the Lindblad equation $\dot{\rho} = -\frac{i}{\hbar}[\hat{H}, \rho]$, where the Hamiltonian of the system could be written in the following form:

$$\hat{H} = \begin{pmatrix} 0 & d^* E_H(t)^* e^{i\omega t} & d^* E_V(t)^* e^{i\omega t} \\ d E_H(t) e^{-i\omega t} & \hbar\omega_0 & 0 \\ d E_V(t) e^{-i\omega t} & 0 & \hbar\omega_0 \end{pmatrix}, \quad (1)$$

where $E_{H(V)}(t)$ is the envelope of the electric field in the light pulse polarized along with the H (V) axis, d is the value of the dipole moment of an optical transition, ω_0 is the transition frequency, and ω is the light frequency. We will use the approximation of infinitely short pulses. In this case

the spontaneous PE experiment could be broken down into the sequence of actions of light pulses with areas $\Theta_{H(V)} = \lim_{t_p \to \infty}(\frac{2}{\hbar}|\mathsf{d}\mathsf{E}_{H(V)}(t)t_p|)$, and temporal evolutions of the density matrix in the absence of the light field. The initial state of the system has a single nonzero density matrix element $\rho_{00} = 1$. We consider the simple spontaneous PE sequence with the first pulse area $\Theta_{H1} = \frac{\pi}{2}$, $\Theta_{V1} = 0$ (fully H-polarized $\frac{\pi}{2}$ pulse) and $\Theta_{H2} = \pi \cos\varphi$, $\Theta_{V2} = \pi \sin\varphi$ (π pulse with linear polarization rotated by the angle φ with respect to H axis). The pulses are separated by the time delay τ.

The polarization components $P_{H(V)}$ of the system could be found as $P_{H(V)} = \mathrm{Tr}(\hat{d}_{H(V)}\rho) = 2\mathrm{Re}(d\rho_{01(02)}(\omega_0, t))$, here $\hat{d}_{H(V)}$ is the dipole moment operator for $|0\rangle \leftrightarrow |H\rangle$ ($|0\rangle \leftrightarrow |V\rangle$) transitions. To calculate the PE signal from the ensemble one has to sum $P_{H(V)}(\omega_0, t)$ over all ω_0. We will consider the Gaussian-shaped inhomogeneously broadened ensemble centered at the light frequency: $\omega_0 = \omega$.

Finally, two linearly polarized components of the PE signal amplitude at $t = 2\tau$ could be obtained in the following form: $P_H \sim \cos^2(\varphi)$, $P_V \sim \sin(\varphi)\cos(\varphi)$.

[1] L. Langer, S. Poltavtsev, I. Yugova, M. Salewski, D. Yakovlev, G. Karczewski, T. Wojtowicz, I. Akimov, and M. Bayer, Access to long-term optical memories using photon echoes retrieved from semiconductor spins, Nat. Photonics **8**, 851 (2014).

[2] I. Solovev, I. Yanibekov, Y. Efimov, S. Eliseev, V. Lovcjus, I. Yugova, S. Poltavtsev, and Y. Kapitonov, Long-lived dark coherence brought to light by magnetic-field controlled photon echo, Phys. Rev. B **103**, 235312 (2021).

[3] M. Salewski, S. Poltavtsev, Y. Kapitonov, J. Vondran, D. Yakovlev, C. Schneider, M. Kamp, S. Höfling, R. Oulton, I. Akimov, A. Kavokin, and M. Bayer, Photon echoes from (In,Ga)As quantum dots embedded in a Tamm-plasmon microcavity, Phys. Rev. B **95**, 035312 (2017).

[4] S. Poltavtsev, I. Solovev, I. Akimov, V. Chaldyshev, W. Lundin, A. Sakharov, A. Tsatsulnikov, D. Yakovlev, and M. Bayer, Long coherent dynamics of localized excitons in (In,Ga)N/GaN quantum wells, Phys. Rev. B **98**, 195315 (2018).

[5] I. Solovev, S. Poltavtsev, Y. Kapitonov, I. Akimov, S. Sadofev, J. Puls, D. Yakovlev, and M. Bayer, Coherent dynamics of localized excitons and trions in ZnO/(Zn,Mg)O quantum wells studied by photon echoes, Phys. Rev. B **97**, 245406 (2018).

[6] A. Splendiani, L. Sun, Y. Zhang, T. Li, J. Kim, C.-Y. Chim, G. Galli, and F. Wang, Emerging photoluminescence in monolayer MoS₂, Nano Lett. **10**, 1271 (2010).

[7] M. Ugeda, A. Bradley, S.-F. Shi, F. Da Jornada, Y. Zhang, D. Qiu, W. Ruan, S.-K. Mo, Z. Hussain, Z.-X. Shen, F. Wang, S. Louie, and M. Crommie, Giant bandgap renormalization and excitonic effects in a monolayer transition metal dichalcogenide semiconductor, Nat. Mater. **13**, 1091 (2014).

[8] R. Lv, J. Robinson, R. Schaak, D. Sun, Y. Sun, T. Mallouk, and M. Terrones, Transition metal dichalcogenides and beyond: Synthesis, properties, and applications of single- and few-layer nanosheets, Acc. Chem. Res. **48**, 56 (2015).

[9] A. Miyata, A. Mitioglu, P. Plochocka, O. Portugall, J.-W. Wang, S. Stranks, H. Snaith, and R. Nicholas, Direct measurement of the exciton binding energy and effective masses for charge carriers in organic-inorganic tri-halide perovskites, Nat. Phys. **11**, 582 (2015).

[10] K. Tanaka, T. Takahashi, T. Ban, T. Kondo, K. Uchida, and N. Miura, Comparative study on the excitons in lead-halide-based perovskite-type crystals CH₃NH₃PbBr₃ CH₃NH₃PbI₃, Solid State Commun. **127**, 619 (2003).

[11] A. Kojima, K. Teshima, Y. Shirai, and T. Miyasaka, Organometal halide perovskites as visible-light sensitizers for photovoltaic cells, J. Am. Chem. Soc. **131**, 6050 (2009).

[12] M. Lee, J. Teuscher, T. Miyasaka, T. Murakami, and H. Snaith, Efficient hybrid solar cells based on meso-superstructured organometal halide perovskites, Science **338**, 643 (2012).

[13] H.-S. Kim, C.-R. Lee, J.-H. Im, K.-B. Lee, T. Moehl, A. Marchioro, S.-J. Moon, R. Humphry-Baker, J.-H. Yum, J. Moser *et al.*, Lead iodide perovskite sensitized all-solid-state submicron thin film mesoscopic solar cell with efficiency exceeding 9%, Sci. Rep. **2**, 591 (2012).

[14] J. Kangand L.-W. Wang, High defect tolerance in lead halide perovskite $CsPbBr_3$, J. Phys. Chem. Lett. **8**, 489 (2017).

[15] K. Steirer, P. Schulz, G. Teeter, V. Stevanovic, M. Yang, K. Zhu, and J. Berry, Defect tolerance in methylammonium lead triiodide perovskite, ACS Energy Lett. **1**, 360 (2016).

[16] M. Antonietta Loiand J. Hummelen, Hybrid solar cells: Perovskites under the sun, Nat. Mater. **12**, 1087 (2013).

[17] M. Hirasawa, T. Ishihara, T. Goto, K. Uchida, and N. Miura, Magnetoabsorption of the lowest exciton in perovskite-type compound $(CH_3NH_3)PbI_3$, Phys. B: Condens. Matter **201**, 427 (1994).

[18] T. Ishihara, Optical properties of PbI-based perovskite structures, J. Lumin. **60-61**, 269 (1994).

[19] N. Kitazawa, Y. Watanabe, and Y. Nakamura, Optical properties of $CH_3NH_3PbX_3$ (X = halogen) and their mixed-halide crystals, J. Mater. Sci. **37**, 3585 (2002).

[20] S. Stranks, G. Eperon, G. Grancini, C. Menelaou, M. Alcocer, T. Leijtens, L. Herz, A. Petrozza, and H. Snaith, Electron-hole diffusion lengths exceeding 1 micrometer in an organometal trihalide perovskite absorber, Science **342**, 341 (2013).

[21] G. Xing, N. Mathews, S. Sun, S. Lim, Y. Lam, M. Graetzel, S. Mhaisalkar, and T. Sum, Long-range balanced electron-and hole-transport lengths in organic-inorganic $CH_3NH_3PbI_3$, Science **342**, 344 (2013).

[22] J. Even, L. Pedesseau, and C. Katan, Analysis of multivalley and multibandgap absorption and enhancement of free carriers related to exciton screening in hybrid perovskites, J. Phys. Chem. C **118**, 11566 (2014).

[23] H. Diab, G. Trippé-Allard, F. Lédée, K. Jemli, C. Vilar, G. Bouchez, V. Jacques, A. Tejeda, J. Even, J.-S. Lauret, E. Deleporte, and D. Garrot, Narrow linewidth excitonic emission in organic-inorganic lead iodide perovskite single crystals, J. Phys. Chem. Lett. **7**, 5093 (2016).

[24] J. Tilchin, D. Dirin, G. Maikov, A. Sashchiuk, M. Kovalenko, and E. Lifshitz, Hydrogen-like Wannier-Mott excitons in single crystal of methylammonium lead bromide perovskite, ACS Nano **10**, 6363 (2016).

[25] K. Galkowski, A. Mitioglu, A. Miyata, P. Plochocka, O. Portugall, G. Eperon, J.-W. Wang, T. Stergiopoulos, S. Stranks, H. Snaith, and R. Nicholas, Determination of the exciton binding energy and effective masses for methylammonium and formamidinium lead tri-halide perovskite semiconductors, Energy Environ. Sci. **9**, 962 (2016).

[26] Z. Yang, A. Surrente, K. Galkowski, N. Bruyant, D. Maude, A. Haghighirad, H. Snaith, P. Plochocka, and R. Nicholas, Unraveling the exciton binding energy and the dielectric constant in single-crystal methylammonium lead triiodide perovskite, J. Phys. Chem. Lett. **8**, 1851 (2017).

[27] Z. Yang, A. Surrente, K. Galkowski, A. Miyata, O. Portugall, R. Sutton, A. Haghighirad, H. Snaith, D. Maude, P. Plochocka, and R. Nicholas, Impact of the halide cage on the electronic properties of fully inorganic cesium lead halide perovskites, ACS Energy Lett. **2**, 1621 (2017).

[28] S. March, C. Clegg, D. Riley, D. Webber, I. Hill, and K. Hall, Simultaneous observation of free and defect-bound excitons in $CH_3NH_3PbI_3$ using four-wave mixing spectroscopy, Sci. Rep. **6**, 39139 (2016).

[29] S. March, D. Riley, C. Clegg, D. Webber, X. Liu, M. Dobrowolska, J. Furdyna, I. Hill, and K. Hall, Four-wave mixing in perovskite photovoltaic materials reveals long dephasing times and weaker many-body interactions than GaAs, ACS Photonics **4**, 1515 (2017).

[30] S. March, D. Riley, C. Clegg, D. Webber, I. Hill, Z.-G. Yu, and K. Hall, Ultrafast acoustic phonon scattering in $CH_3NH_3PbI_3$ revealed by femtosecond four-wave mixing, J. Chem. Phys. **151**, 144702 (2019).

[31] B. Bohn, T. Simon, M. Gramlich, A. Richter, L. Polavarapu, A. Urban, and J. Feldmann, Dephasing and quantum beating of excitons in methylammonium lead iodide perovskite nanoplatelets, ACS Photonics **5**, 648 (2018).

[32] T. Kondo, S. Iwamoto, S. Hayase, K. Tanaka, J. Ishi, M. Mizuno, K. Ema, and R. Ito, Resonant third-order optical nonlinearity in the layered perovskite-type material $(C_6H_{13}NH_3)_2PbI_4$, Solid State Commun. **105**, 503 (1998).

[33] J. Ishi, H. Kunugita, K. Ema, T. Ban, and T. Kondo, Time-to-space conversion of Tbits/s optical pulses using a self-organized quantum-well material, Appl. Phys. Lett. **77**, 3487 (2000).

[34] J. Ishi, H. Kunugita, K. Ema, T. Ban, and T. Kondo, Influence of exciton-exciton interactions on frequency-mixing signals in a stable exciton-biexciton system, Phys. Rev. B **63**, 073303 (2001).

[35] A. V. Trifonov, S. Grisard, A. N. Kosarev, I. A. Akimov, D. R. Yakovlev, J. Höcker, V. Dyakonov, and M. Bayer, Photon echo polarimetry of excitons and biexcitons in a $CH_3NH_3PbI_3$ perovskite single crystal, ACS Photonics **9**, 621 (2022).

[36] C. Quarti, C. Katan, and J. Even, Physical properties of bulk, defective, 2D and 0D metal halide perovskite semiconductors from a symmetry perspective, J. Phys. Materials **3**, 042001 (2020).

[37] V. Yudin, M. Lozhkin, A. Shurukhina, A. Emeline, and Y. Kapitonov, Photoluminescence manipulation by ion beam irradiation in $CsPbBr_3$ halide perovskite single crystals, J. Phys. Chem. C **123**, 21130 (2019).

[38] G. Garcia-Arellano, G. Trippé-Allard, L. Legrand, T. Barisien, D. Garrot, E. Deleporte, F. Bernardot, C. Testelin, and M. Chamarro, Energy tuning of electronic spin coherent evolution in methylammonium lead iodide perovskites, J. Phys. Chem. Lett. **12**, 8272 (2021).

[39] N. I. Selivanov, A. O. Murzin, V. I. Yudin, Y. V. Kapitonov, and A. V. Emeline, Counterdiffusion-in-gel growth of high optical and crystal quality $MAPbX_3$ (MA = CH_3NH_3+, X = I-, Br-) lead-halide perovskite single crystals, arXiv:2104.03175.

[40] N. Selivanov, A. Samsonova, R. Kevorkyants, I. Krauklis, Y. Chizhov, B. Stroganov, M. Triantafyllou-Rundell, D. Bahnemann, C. Stoumpos, A. Emeline, and Y. Kapitonov, Hybrid organicinorganic halide post-perovskite 3-cyanopyridinium lead tribromide for optoelectronic applications, Adv. Funct. Mater. **31**, 2102338 (2021).

[41] N. Selivanov, Y. Rozhkova, R. Kevorkyants, A. Emeline, and D. Bahnemann, The effect of organic cations on the electronic, optical and luminescence properties of 1d piperidinium, pyridinium, and 3-hydroxypyridinium lead trihalides, Dalton Transactions **49**, 4390 (2020).

[42] Y. Yamada, T. Yamada, L. Phuong, N. Maruyama, H. Nishimura, A. Wakamiya, Y. Murata, and Y. Kanemitsu,

Dynamic optical properties of $CH_3NH_3PbI_3$ single crystals as revealed by one- and two-photon excited photoluminescence measurements, J. Am. Chem. Soc. **137**, 10456 (2015).

[43] A. Murzin, N. Selivanov, V. Kozlov, I. Ryzhov, T. Miyasaka, A. Emeline, and Y. Kapitonov, Photoluminescence excitation spectroscopy of defect-related states in $MAPbI_3$ perovskite single crystals, Adv. Opt. Mater. **9**, 2001327 (2021).

[44] O. Lozhkina, V. Yudin, A. Murashkina, V. Shilovskikh, V. Davydov, R. Kevorkyants, A. Emeline, Y. Kapitonov, and D. Bahnemann, Low inhomogeneous broadening of excitonic resonance in $MAPbBr_3$ single crystals, J. Phys. Chem. Lett. **9**, 302 (2018).

[45] S. Poltavtsev, M. Salewski, Y. Kapitonov, I. Yugova, I. Akimov, C. Schneider, M. Kamp, S. Höfling, D. Yakovlev, A. Kavokin, and M. Bayer, Photon echo transients from an inhomogeneous ensemble of semiconductor quantum dots, Phys. Rev. B **93**, 121304 (2016).

[46] N. Onoda-Yamamuro, T. Matsuo, and H. Suga, Calorimetric and ir spectroscopic studies of phase transitions in methylam- monium trihalogenoplumbates (ii), J. Phys. Chem. Solids **51**, 1383 (1990).

[47] M. Baranowski, K. Galkowski, A. Surrente, J. Urban, L. Klopotowski, S. Mackowski, D. Maude, R. Ben Aich, K. Boujdaria, M. Chamarro, *et al.*, Giant fine structure splitting of the bright exciton in a bulk $MAPbBr_3$ single crystal, Nano Lett. **19**, 7054 (2019).

[48] J. Gordon, C. Wang, C. Patel, R. Slusher, and W. Tomlinson, Photon echoes in gases, Phys. Rev. **179**, 294 (1969).

[49] S. Poltavtsev, Y. Kapitonov, I. Yugova, I. Akimov, D. Yakovlev, G. Karczewski, M. Wiater, T. Wojtowicz, and M. Bayer, Polarimetry of photon echo on charged and neutral excitons in semiconductor quantum wells, Sci. Rep. **9**, 5666 (2019).

[50] Ia. A. Babenko, I. A. Yugova, S. V. Poltavtsev, M. Salewski, I. A. Akimov, M. Kamp, S. Höfling, D. R. Yakovlev, and M. Bayer, Studies of photon echo from exciton ensemble in (In,Ga)As quantum dots, J. Phys.: Conf. Ser. **951**, 012029 (2018).